IEEE Access
Multidisciplinary | Rapid Review | Open Access Journal

Received February 12, 2020, accepted February 27, 2020, date of publication March 3, 2020, date of current version March 12, 2020.

Digital Object Identifier 10.1109/ACCESS.2020.2977853

Simulation of an NSGA-III Based Fireball Inner-Temperature-Field Reconstructive Method

XUE BING[1,2], HAO XIAOJIAN[1,2], LIU XUANDA[1,2], HAN ZIQI[3], AND ZHOU HANCHANG[1,4]

[1]Science and Technology on Electronic Test and Measurement Laboratory, North University of China, Taiyuan 030051, China
[2]School of Instrument and Electronics, North University of China, Taiyuan 030051, China
[3]Beijing Jinghang Computation & Communication Research Institute, Beijing 100000, China
[4]School of Information and Communication Engineering, North University of China, Taiyuan 030051, China

Corresponding author: Hao Xiaojian (haoxiaojian@nuc.edu.cn)

This work was supported in part by the Open Fund of State Key Laboratory of Deep Buried Target Damage under Grant DXMBJJ2018-09, and in part by the Pre-Research Field Foundation of Equipment Development Department of China under Grant 61400030202.

ABSTRACT For the inner-temperature-field reconstruction of a fireball, a detecting method was proposed, using multi-channel visible spectral remote sensing theory. In our proposed method, the reconstructive algorithm based on multi-channel-detection was considered as a multi-objective optimization problem (MOOP), and a fast non-dominated sorting genetic algorithm based on reference-point strategy (NSGA-III) was employed as the solution of this problem. Besides, a so-called ambient pressure operator, based on the unique detecting model, was proposed and employed during the iteration process, for dynamic genetic parameter adjustment. To verify some performance of our proposed method, several numerical reconstructive simulations were carried out, from simple GA to NSGA-III, using several artificial 2-D virtual data, with different kinds of crossover and mutation functions. The simulation results show that, limited to our problems, the NSGA-III can effectively reconstruct different 2-D data, by a fixed crossover rate and a dynamic mutation rate under the proposed ambient pressure operator and an adaptive mutation rate function. The algorithm, limited to the field-reconstruction, also performs well on stability, but still has some deficiencies to be optimized.

INDEX TERMS Field reconstruction, MOOP, NSGA-III, ambient pressure operator.

I. INTRODUCTION

In order to obtain the inner-temperature distribution of a fireball, several non-contact and contact detection method have been developed. Our work in fund project is using several ultra-high-speed visible spectral cameras to gain multi-channel images of the target projection, and then using the images to reconstruct the inside temperature field, where the 3-D reconstructive algorithm is urgently required after the image acquisition. Our currently works were, besides the development of the optical detection system, proposing a NSGA-III based reconstructive method, simplifying the projection model and using several artificial 2-D virtual data to prove the effectiveness of our algorithm. In this section, the optical detection system, multi-channel-images based reconstructive system [1], and the motivation of choosing NSGA-III [2], [3] will be introduced.

A. THE VISIBLE LIGHT DETECTION SYSTEM FOR FIREBALL

The detection system proposed in our project for fireball inner temperature field, was considered having several high-speed visible spectral cameras. As is shown in figure 1, these cameras shall be implemented around the blast fireball, outside the dangerous distance, to obtain the projections from different directions of the fireball, geometric optical theory followed, and the storage module will record each frame of the projection data, collected in a certain direction. After sampling for a period of time, reprocess the collected images, and a reconstructive field will finally be available. There are two important hypotheses in the detection system, and both play important roles in the entire reconstruction theory.

Firstly, as is shown in figure 2, each camera in our detection system, must have different trigger and storage time, which

The associate editor coordinating the review of this manuscript and approving it for publication was Paul Yoo.

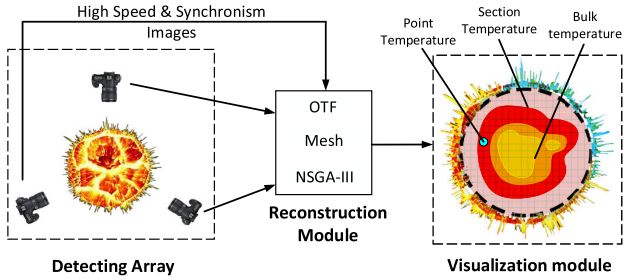

FIGURE 1. Visible light detection and reconstruction system with several cameras.

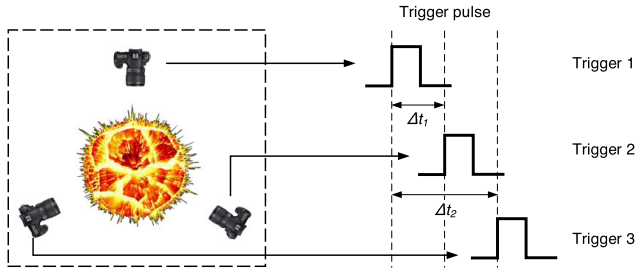

FIGURE 2. Δt of trigger pulse between different detecting channels.

could be efficiently reduced by modern and expensive techniques. However, when developing the reconstructive algorithm, assuming that the camera array having a sufficiently high sampling frequency and synchronization hypothesis is quite helpful, by which images from different cameras in similar frames can consider to be captured at a same time.

The second hypothesis is the simplification of the optical transfer function (OTF), which we call it Temperature-Intensity relation, converting the inner temperature to the gathered projection. The actual overall relation, which considered quite complicated, is currently simplified as three sub relations, as is briefly described in figure 3, which are thermal excitation of elements, reduction of the radiation and receiving property of our multi-channel sensors.

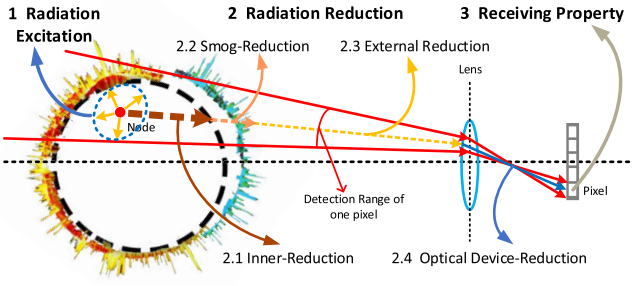

FIGURE 3. Three main process in the OTF.

In the second hypothesis above, shown in figure 3, based on thermal radiation theory, we consider that each position inside a transient fireball must have a determined temperature message, exciting the elements contained in this position and generating radiation with special spectrum [4], [5]. So, we can define formulation (1) to represent this process.

$$I_{e,(x,y,z)} = f_{excitation}\left(\Theta_{(x,y,z)}, \varepsilon_\lambda\right). \tag{1}$$

where $\Theta_{(x,y,z)}$ represents the temperature of one node inside the fireball area, whose coordinate value are (x, y, z) and emissivity is ε_λ. By a certain function $f_{excitation}$ based on black-body radiation law, the emissive thermal radiation $I_{e,(x,y,z)}$ can finally be acquired.

In the next place, considering one of the radiation lines generated, four environmental conditions were considered, that are propagation inside the fireball, propagation through the vapor or smoke, propagation in the atmosphere, and propagation through the optical devices, causing the attenuation of the radiation energy. This attenuation process [6] can be defined as formulation (2).

$$I_{a,(x,y,z)} = f_{attenutation}\left(I_{e,(x,y,z)}, H\right). \tag{2}$$

where H represents the set of different attenuation coefficients. The intensity of radiation after attenuation $I_{a,(x,y,z)}$ can be calculated through the attenuation process $f_{attenutation}$.

Finally, the rest radiation I_a will be converted according to the photoelectric conversion properties [7], [8], and $f_{photoreception}$ as formulation (3) can define the relation between the gray level D_{gray} and the rest light intensity I_a.

$$D_{gray} = f_{photoreception}(I_a, \Delta t). \tag{3}$$

where Δt is the integration time of pixels.

From a different point, the gray level of one pixel might correspond, not to the temperature of a single node, but to the temperature of multiple nodes based on geometrical optics as figure 4. This relation plays an significant role in the reconstructive system which means the error generated in one pixel, must mainly come from the value of points related to this certain pixel.

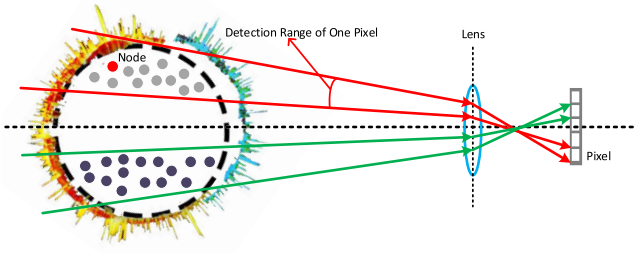

FIGURE 4. Related points of pixels inside the fireball.

As a result, we can achieve expressions (4), describing the gray-level $D_{(m.n)}$ of each pixel in one entire image located at (m, n). So the gray level of the whole image can be described as D_i, the set of all $D_{(m.n)}$ in the photographic film of channel i.

$$\begin{cases} D_{(m.n)} = \sum\limits_{V} f_{photoreception}\left(I_{a,(x,y,z)}, \Delta t\right) \\ D_i = \left\{D_{(i,m,n)} \,|\, 1 \le m \le M, 1 \le n \le N\right\} \end{cases} \tag{4}$$

where any $(x, y, z) \in V$ and V is the corresponding space area of No.(m, n) pixel in one detecting channel, i.e. $(m, n) \rightarrow V$.

Summarize from formulation (1) to (4), the temperature of an inner point and the change of pixel gray level can be generally described as a general formulation (5).

$$D_i = \left\{ D_{(i,m,n)} \left| \sum_V f_{trans} \left(\Theta_{(x,y,z)}, \varepsilon_\lambda, H, \Delta t \right) \right. \right\} \tag{5}$$

B. MOOP BASED RECONSTRUCTIVE METHOD

Based on the images collected in section 1.1, the field reconstructive system can be described as the schematic shown in figure 5.

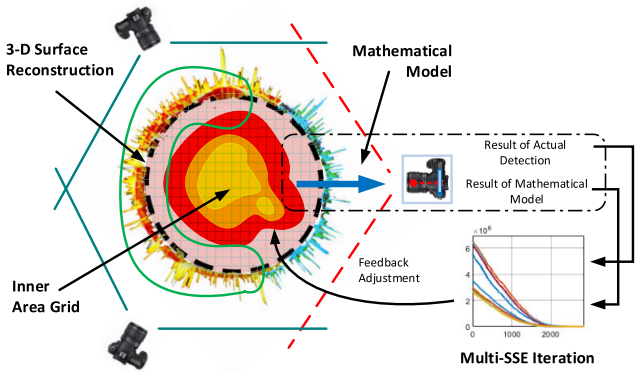

FIGURE 5. The reconstrutive theory based on multi-channel detection and MOOP.

At first, coordinate range of the fireball area should be calculated by surface 3D reconstructive algorithm according to the multi-channel images. The area calculated can further be divided into a fixed grid, with the initial temperature information given to the grid node. Then, by using the relation defined in expressions (5) and (6), multi-channel projections of the artificial temperature field above, can be calculated. Numerical difference between the projections calculated and the projections sampling by the camera array, must exist and could be calculated as formulation (7). Iterative method is chosen to adjust the temperature value of a node inside the inner fireball mesh, aiming at reducing the error calculated by the sum of squared errors (SSE) of all pixels in one image, between the calculated projection and the collected projection. By using this kind of SSE, one SSE can represents the fitness of the current iteration result in a certain detection channel, and the purpose of iteration is to find the best numerical temperature field solution, fitting all channels' SSE well, which is similar to a multi-objective optimization problem (MOOP) [9], [10] and is suitable for many multi-objective evolution algorithms (MOEA) [11], [12]. Finally, the best solution found in the process of iteration, will be the reconstructed result of the fireball inner temperature field.

II. IMPLEMENT OF NSGA-III TO THE RECONSTRUCTIVE ALGORITHM

Since the multi-channel-projection based field reconstructive method has been classified as MOOP, NSGA-III is chosen to solve this problem [13]. There are two significant points in implement of the algorithm. The first is the simplification of the detection model to build a simple mathematical model. The second is the combination of NSGA-III and the simplified model.

A. SIMPLIFIED MATHEMATICAL MODEL

In the primary stage of the reconstructive project, it is difficult to verify the reconstructive method is actually work, without having real detection data. So, a simplified mathematical model was designed to simulate the detection process, with three main concepts.

The first concept is trying 2-D simulations before 3-D simulations. Same to the 3-D situation, 2-D simulation can keep the corresponding relationship between the projection and internal value, only having difference in the dimension of variables in calculation. Guided by this theory, virtual 2-D fireball data and virtual visible spectral camera array was randomly created.

The second concept is the generation of 2-D fireball data sets. The fireball may have several high temperature regions inside the explosion area. So, we randomly choose three centers and three radii, generating several virtual fireball data sets, as is shown in Fig 6.

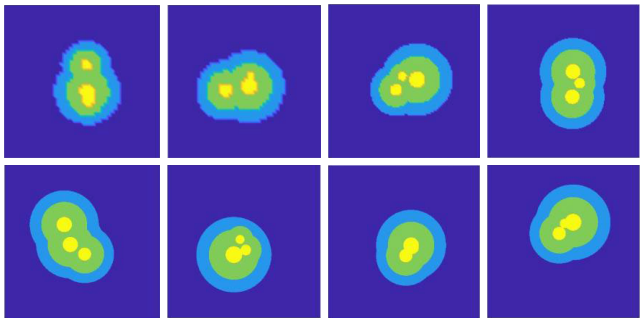

FIGURE 6. Several aritificial 2-D fireball iamges randomly generated by program.

The third concept is using the principle of pinhole imaging, one of the simple but frequently-used OTF, in calculating projections. In 2-D situation, for one virtual pixel in figure 7, two vectors can be calculated by one virtual focus and the two boundary points of the pixel.

In the 2-D vector space, the two vectors $\overrightarrow{P_{1,i}O_i}$ and $\overrightarrow{P_{2,i}O_i}$ can be the base vectors as they are linearly independent, and all points can be represented by the two vectors as formulation (6), where the virtual focus point can be described as $O_i = \begin{bmatrix} o_x & o_y \end{bmatrix}$, one random object point can be described as $P = \begin{bmatrix} p_x & p_y \end{bmatrix}$, and the neighbouring two boundary points of one pixel are $P_{1,i} = \begin{bmatrix} x_{1,i} & y_{1,i} \end{bmatrix}$ and $P_{2,i} = \begin{bmatrix} x_{2,i} & y_{2,i} \end{bmatrix}$.

$$\begin{cases} \overrightarrow{P_{1,i}O_i} = \begin{bmatrix} x_{1,i} - o_x & y_{1,i} - o_y \end{bmatrix}^T \\ \overrightarrow{P_{2,i}O_i} = \begin{bmatrix} x_{2,i} - o_x & y_{2,i} - o_y \end{bmatrix}^T \end{cases} \tag{6}$$

According to the principle of pinhole imaging, the point is judged to project towards the pixel, when two coefficients $k_{1,i}$

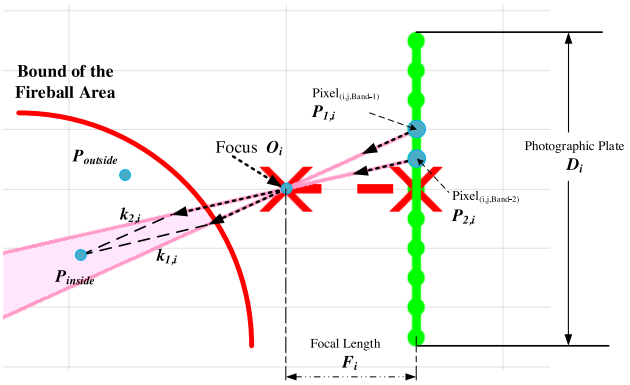

FIGURE 7. The vectorial representation of pinhole iamging.

and $k_{2,i}$, derived from formulation (7-9), are both positive.

$$\begin{cases} \overrightarrow{PO_i} = \begin{bmatrix} k_{1,i} & k_{2,i} \end{bmatrix} \begin{bmatrix} \overrightarrow{P_{1i}O_i} & \overrightarrow{P_{2i}O_i} \end{bmatrix}^T \\ \quad = \begin{bmatrix} k_{1,i} & k_{2,i} \end{bmatrix} \begin{bmatrix} x_{1,i} - o_x & y_{1i} - o_y \\ x_{2,i} - o_x & y_{2i} - o_y \end{bmatrix} \\ \overrightarrow{PO_i} = \begin{bmatrix} p_x & p_y \end{bmatrix} - \begin{bmatrix} o_x & o_y \end{bmatrix} \\ \quad = \begin{bmatrix} p_x - o_x & p_y - o_y \end{bmatrix} \end{cases} \tag{7}$$

$$\begin{bmatrix} p_x - o_x \\ p_y - o_y \end{bmatrix} = \begin{bmatrix} x_{1,i} - o_x & x_{2,i} - o_x \\ y_{1,i} - o_y & y_{2,i} - o_y \end{bmatrix} \begin{bmatrix} k_{1,i} \\ k_{2,i} \end{bmatrix} \tag{8}$$

$$\begin{bmatrix} k_{1,i} \\ k_{2,i} \end{bmatrix} = \begin{bmatrix} x_{1,i} - o_x & x_{2,i} - o_x \\ y_{1,i} - o_y & y_{2,i} - o_y \end{bmatrix}^{-1} \begin{bmatrix} p_x - o_x \\ p_y - o_y \end{bmatrix} \tag{9}$$

Based on the concepts above, figure 8 shows a 2-D 10-channel virtual detection system, with 40 pixels, implemented around a random 2-D artificial fireball.

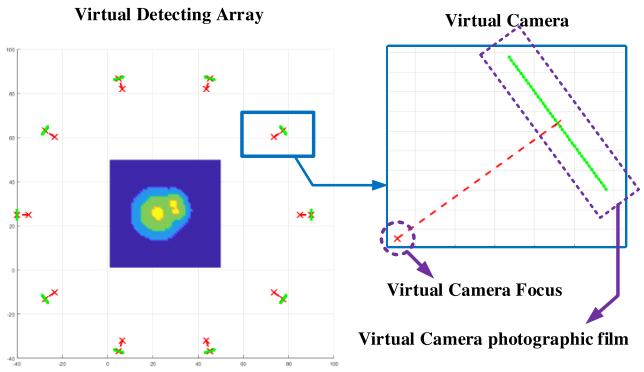

FIGURE 8. Virtual multi-channel imaging system.

B. APPLICATION OF NSGA-III IN THE RECONSTRUCTIVE ALGORITHM

In the optical model of the detection system, the Temperature-Intensity relation might quite complex, and maybe quite difficult to solve the backward relation. So genetic algorithm (GA) was chosen, only using the forward relation to participate iteration. Different from the simple genetic algorithm, NSGA use non-dominated sorting [14], [15] as the elitist strategy to choose better individuals in iteration, and drive the iteration based on GA theory [16], [18]. From NSGA to NSGA-III, population diversity of individuals has been taken into consideration in NSGA-II, and furthermore, NSGA-III uses a reference point association to effectively overcome this problem. The application of NSGA-III can be described as what is shown in figure 9.

*Step*1. Load an artificial 2-D fireball and set the virtual camera array by the given parameters, like what is shown in figure 8, which automatically generated in MATLAB by our own designed program. Then use the OTF virtual pinhole-imaging OTF as figure(7) and equations(7-9), to generate the standard projections set D_s.

*Step*2. Use projections generated to produce a mean back-projection data $\overline{Ps}$, and implement a fixed mutation rate $p_{mutation}$ on random location (x, y) of $\overline{Ps}$ to produce one initial individual P by equations (10).

$$P(x, y) = \overline{Ps}(x, y) \times (1 + p_{mutation}) \tag{10}$$

where i represents the number of one channel, ranging from 1 to n, and mean back-projection $\overline{Ps}$ can be calculated as below.

$$\overline{Ps} = \frac{1}{n} \sum_{i=1}^{n} D_s(i) \tag{11}$$

*Step*3. Calculate each channel's projection D_{prj} of each individual P with equations (12).

$$D_{prj}(i, j) = \sum_{\substack{j \to V \\ x,y \in V}} f_{trans,node}\left(P_{(x,y)}, \varepsilon_\lambda, H, \Delta t\right) \tag{12}$$

Compare D_{prj} with standard projections D_s in the first step, to get $AE(i, j)$ and $SE(i, j)$ matrix with equations (13), where i represents the number of one channel and j represents the number of one pixel in channel i.

$$\begin{cases} AE(i, j) = \left| D_{prj}(i, j) - D_s(i, j) \right| \\ SE(i, j) = \left(D_{prj}(i, j) - D_s(i, j) \right)^2 \end{cases} \tag{13}$$

*Step*4. Also, as is shown in figure 9, generate child-group by crossover operator and mutation operator, two basic GA operators. During the mutation, a linear mutation rate function [19] was used to control the number of mutation nodes, in order to make the algorithm being adaptive [20], [21]. The mutation rate p_m could be calculated as equations (14).

$$p_m = \frac{p_n}{N} \tag{14}$$

where N is the number of objects (i.e. number of detective channels in this paper), p_n can be calculated as follows.

$$p_n = p + (t - 1) \times \frac{1 - p}{t_m - 1} \tag{15}$$

where t and t_m are the current and maximum generation, respectively; p is a fixed real number, and in this paper p can be given as follows.

$$p = \frac{1}{5} N \tag{16}$$

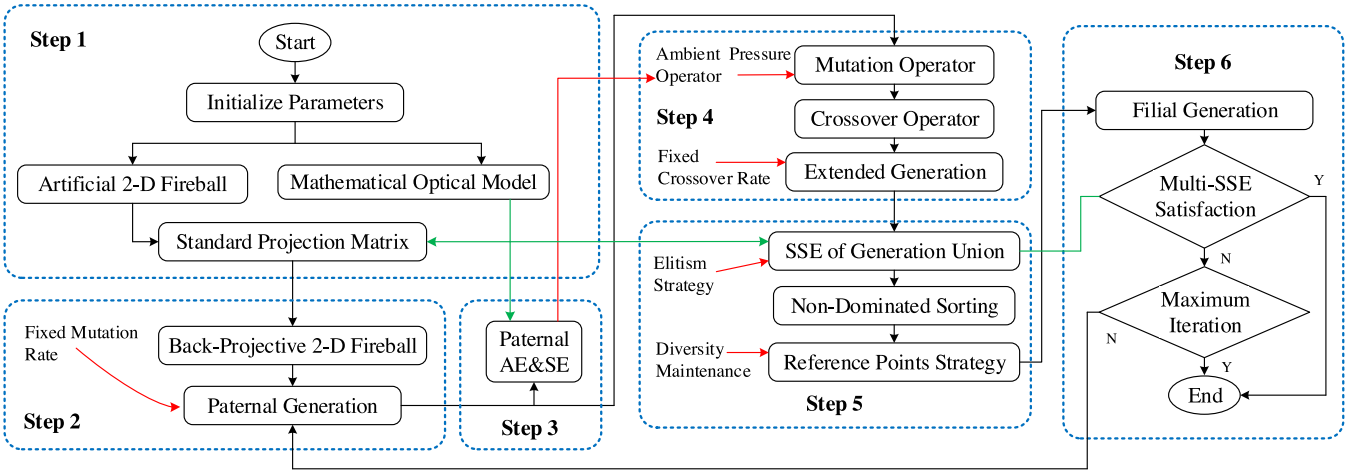

FIGURE 9. Application of NSGA-III in the field reconstructive system.

In order to control the intensity of the mutation, we proposed an ambient pressure operator based on the D-value between $D_{prj}(i,j)$ and $D_s(i,j)$ of the individuals in paternal generation. The aim of development of this operator, based on two theory. On the one hand, the final individuals must be similar to the mean of back-projections of each detecting channels, and all individuals in the iteration can gradually approach to the best individual along the curve, constructed by origin point and fitness point of back-projections' mean value, in this high dimension MOOP. On the other hand, though, the mutation position and mutation value should be and can be controlled by the current error between calculated and observed values, though they are generated by the current mutation rate.

The generation of this proposed ambient pressure operator is described as below.

Firstly, the number of nodes under mutation N_m is controlled by the basic nodes' number N_p and the mutation rate in this generation. The mutation number $N_m\,(i,j)$, in the corresponding region of pixel j of channel i, can be calculated by $N_p(i,j)$, the total number of nodes in the corresponding region of the pixel, and p_m, the mutation rate in the current generation, as formulation (17).

$$N_m\,(i,j) = N_p(i,j) \times p_m \tag{17}$$

Next, when considering the construction of the mutation value, the more error, the more mutation value. As equation (18), both the D-value between $D_{prj}(i,j)$ and $D_s(i,j)$, and a real number K are used to control the size of the mutation corresponding to pixel j of channel i. Besides, the direction of the mutation is defined as the reverse of the D-value. At last, average distribute the mutation value to $N_m\,(i,j)$ nodes.

$$V_m\,(i,j) = -\frac{D_{prj}(i,j) - D_s(i,j)}{K \times N_m\,(i,j)} \tag{18}$$

The real number K is recommended in this paper as follow. This recommended value can restrict the total mutation value to less than 1, which corresponding to a certain pixel, making individuals can converge steadily along, floating in a small range near the mean back-projection $\overline{Ps}$.

$$K = \sum_j AE(i,j) \tag{19}$$

Meanwhile, a fixed rate from experience was chosen as follow to control the number of nodes under crossover process.

$$p_c = 0.7 \tag{20}$$

The results of different P_c values were tested as is shown in figure 10. From figure 10(a), the algorithm can converge to the same value with different Pc and other same parameters. From figure 10(b), when set $P_c = 0.7$, the algorithm can converge a little bit faster than other values. So,$P_c = 0.7$ was chosen as a primary recommended crossover rate from experience.

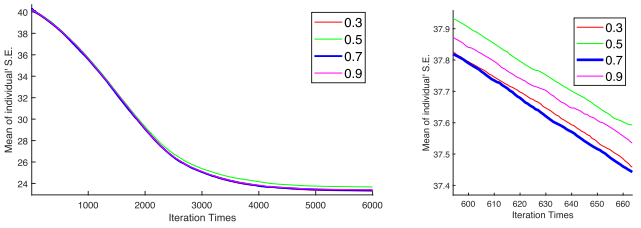

(a) Iteration with different P_c values (b) Rate of convergence in detail

FIGURE 10. Comparison between results of different P_c values.

It is worth noting that the nodes under both crossover and mutation process are randomly generated in the range of the virtual fireball region, which is quite different from the method given in Jakub's paper [16], where all points in related region are chosen to participate in the iteration, as is shown in figure 11(a), which may lead to both the increase of operation and the rise of error. In the proposed fireball

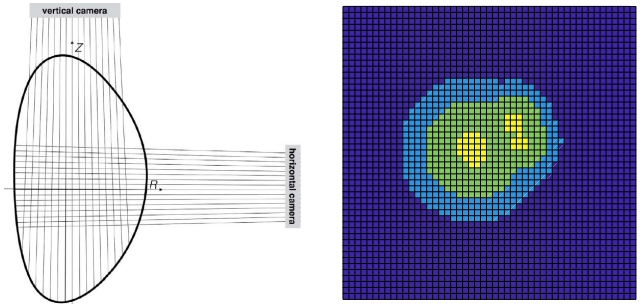

(a) Jakub's whole region method (b) Proposed related region method

FIGURE 11. Difference between Jakub's and proposed method.

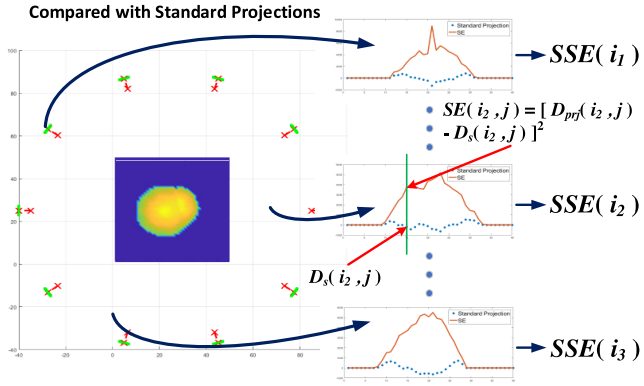

FIGURE 12. Generation of each detecting channel' SSE.

reconstructive system, 3-D surface reconstructive technique, obtained easily on open source library, is introduced to generate the coordinates of the reconstructive area, which can guide the division of finite elements and constrain the region of iteration as figure 11(b).

*Step*5. After the basic genetic process, by merging both child-group and parent-group into one group, and achieving the SE matrix by step 3, as figure 12, the SSE matrix of any individual, inside the united group, can easily be acquired.

The SSE value of individual m towards channel i, i.e. $sse\ (m, i)$, can be achieved by formulation (21).

$$sse\ (m, i) = \sum_{j} SE(m, i, j) \tag{21}$$

where j is the serial number of pixels corresponding to channel i, and the structure of SSE matrix (i.e. SSE_{sort}) is as follow.

$$SSE_{sort} = \begin{bmatrix} sse_{11} & sse_{12} & \cdots & sse_{1N} \\ sse_{21} & sse_{22} & \cdots & sse_{2N} \\ \vdots & \vdots & \ddots & \vdots \\ sse_{M1} & sse_{M2} & \cdots & sse_{MN} \end{bmatrix} \tag{22}$$

SSE_{sort} is an $M \times N$ matrix, where M is the number of individuals and N represents the number of channels. Any row of (i.e. $SSE_{sort}(m, :)$ as below) represents this individual's fitness to each projection channel.

$$SSE_{sort}(m, :) = \begin{bmatrix} sse_{m1} & sse_{m2} & \cdots & sse_{mN} \end{bmatrix} \tag{23}$$

As a result, non-dominated sorting strategy could be used to elect elite individuals from the united groups, based on the multi-fitness vectors (i.e. matrix SSE_{sort}).

In the process of electing elite individuals, firstly, the reference-points association is implemented to keep the diversity of the current population [22]–[24]. In order to construct the reference points in the N-dimensional multi-fitness-vector domain, linear hyperplane method was introduced, whose expression can be described as equation (24).

$$x_1 + x_2 + \cdots x_{N-1} + x_N = a \tag{24}$$

where N is the dimension of the whole multi-fitness-vector space. The constant a can briefly be defined as 1, because that all the vectors above need to be standardized by multi-dimensional coordinate translation (i.e. equations (24)), and multi-dimensional normalization as equations (25).

$$\begin{cases} T = \begin{bmatrix} m_1 & m_2 & \cdots & m_N \end{bmatrix}_{1\times N} \\ m_i = \min \begin{bmatrix} sse_{1i} \\ sse_{2i} \\ \vdots \\ sse_{Mi} \end{bmatrix} \\ U = SSE_{sort} - \begin{bmatrix} 1 \\ 1 \\ \vdots \\ 1 \end{bmatrix}_{M\times 1} \times T \end{cases} \tag{25}$$

where m_i is the minimum value of column i in operator matrix T and T is an $1 \times N$ matrix of the each channel's minimum value and UT is an $M \times N$ matrix, translated from SSE_{sort} by the row matrix T constructed by m_i in all dimension of the fitness.

The elements in UT can be recognized as ut_{ij} where i represents the channels and j represents the individuals. By selecting the maximum value of each column in UT to form the normalized parameter matrix, the normalization of matrix UT is realized, and the standardization of SSE_{sort} is finally completed. The process is described as equations(25).

$$\begin{cases} N = \begin{bmatrix} \frac{1}{mut_1} & \frac{1}{mut_2} & \cdots & \frac{1}{mut_N} \end{bmatrix}_{1\times N} \\ mut_i = \max \begin{bmatrix} ut_{1i} \\ ut_{2i} \\ \vdots \\ ut_{Mi} \end{bmatrix} \\ SSE_{STD} = UT \cdot \left(\begin{bmatrix} 1 \\ 1 \\ \vdots \\ 1 \end{bmatrix}_{M\times 1} \times N \right) \end{cases} \tag{26}$$

where operator matrix N saves reciprocal values of all channels' maximum SSE value. After dividing the columns of N by the maximum of each channel, the SSE matrix under normalization (i.e. SSE matrix standardized, SSE_{STD}) can easily achieved.

After achieving the SSE_{STD} matrix, in order to keep the diversity of individuals' distribution, try the best to relate at least one individual to each reference point, as is shown in figure 13, by comparing the distance between each reference vector with each fitness vector. The reference vector above is generated by the original point and reference points on the N-dimensional reference hyper-plane which constructed by equation (23).

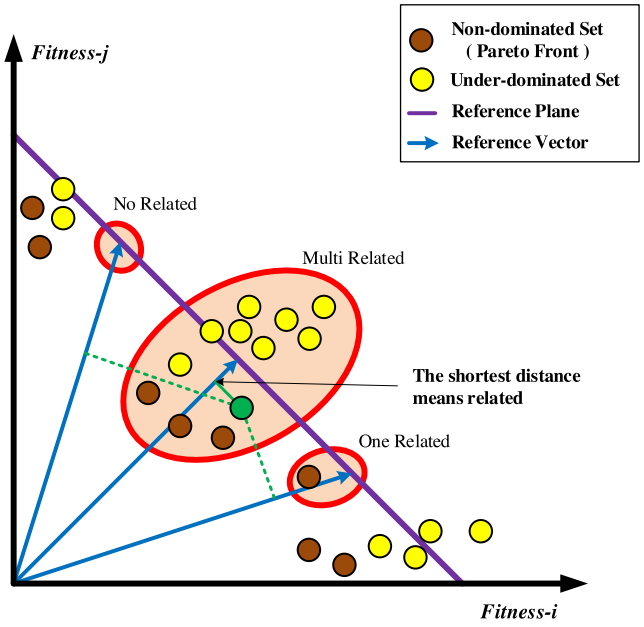

FIGURE 13. Three relative conditions of individuals and reference points.

The distance vector $d_{M,i}$, representing all fitness vectors towards one reference vectors can be calculated as equations (27), according to the point to vector distance theory.

$$d_{M,i} = \frac{1}{|ref_i|} SSE_{STD} \times ref_i^T \tag{27}$$

In the equations above, SSE_{STD} is an $M \times N$ matrix, ref_i is one of the vector on the reference plane, defined as the equation (28) below.

$$ref_i = \begin{bmatrix} x_{i,1} & x_{i,2} & \cdots & x_{i,N} \end{bmatrix}_{1\times N} \tag{28}$$

There are three conditions while counting the number of related individuals as figure 13, and we try to realize that one reference vector only have one related vector. One of the useful solutions is using priority level, where non-dominated individuals is firstly taken into consideration, randomly select one individual from individuals related to a certain reference vector. If the number of individuals remain is not enough, we go back to the non-dominated sets removing in the former step, and randomly pick out several individuals. After that, if the individuals' number is still not enough, we have no choice but picking out individuals in under-dominated sets.

Figure 14 shows the Pareto Front of the individuals during the iteration under a 10-channels reconstruction simulation, where the fitness of all individuals were separated with several 2-D or 3-D fitness by projection for visualization. The individuals were forming several niche, which could be observed easily during the iteration, which may be caused by the normalized reference points.

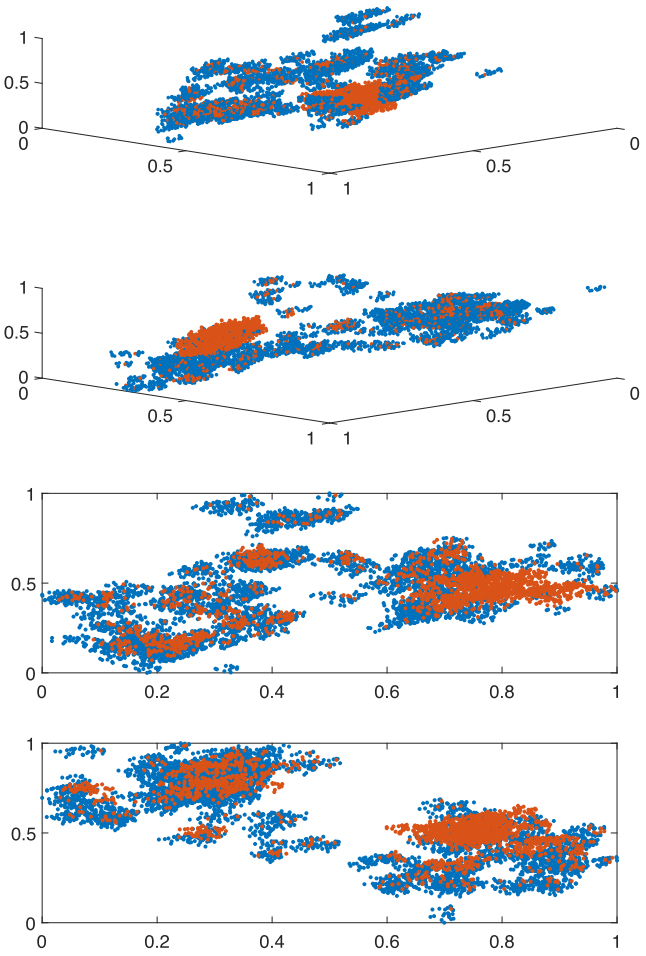

FIGURE 14. Visualization of 10-D Fitness (where blue points represent Pareto Front).

*Step*6. The individuals picked out from the merging paternal group make up the filial elite set. The elite set, when their SSE matrix cannot satisfy our expectation, will be sent back to step 2 as the paternal individuals, to carry out a new round of iteration. The iteration process shall stop automatically only when the error of the individuals can satisfy the requirements or when the number of iterations is out of maximum bound.

III. SIMULATION RESULTS

Based on the simplified mathematical model and the reconstructive strategy above, several numerical experiments have been implemented, using the same projection mathematical

model (i.e. pinhole imaging model with the same relative parameters) and same size of virtual fireball data, but under other different parameter conditions. The simulative tests of the proposed reconstructive method contain four different situations.

All of our simulations were carried out on a personal computer with a Intel(R) Core(TM) i7-8700K CPU, Kingston DDR4 3600Hz 32G RAM. The software platform are Windows 10 professional and MATLAB R2019a.

A. COMPARISON BETWEEN GA, NSGA AND NSGA-III

The same virtual fireball and the same position parameters of all detecting channels, but different reconstructive theory and different number of the detecting channel were employed, in order to show that NSGA-III works completely better than simple GA and basic NSGA in this special MOOP. The reconstructive results of same artificial data by different method are compared in figure 15 with rising number of channels. From the visual qualitative analysis shown in figure 15, NSGA-III do have the obviously better reconstructive results than basic NSGA and Simple Genetic Algorithm. This may mainly because of the reference points method in NSGA-III, by which the diversity of individuals can stably be maintained and the local optimal solutions during the iteration can effectively be avoided.

B. COMPARISON BETWEEN FIXED RATE METHOD AND PROPOSED METHOD

Iterations with fixed parameters and proposed dynamic control method were tested under the same condition. The mutation rate has effect on both value and number of the individuals as equation (17). When using the same parametric condition and the same target, the mutation rate have a great effect on the convergent speed as is shown in figure 16. The explanation of this phenomenon is inferred as the influence of both the dynamic rate and the proposed operator. The proposed operator has the ability in applying more adjustment to the place with larger error.

C. COMPARISON BETWEEN DIFFERENT NUMBER OF CHANNELS

Based on the fact that NSGA-III has been proved to be the most suitable method in this multi-channel reconstructive problem, the same virtual data and different number of channels were used, to test what may be caused by different number of detective channel. The results of simulations with different number of channels are shown in figure 17, where the same color represents the same value. Also from the visual qualitative analysis, reconstructive results become better with the increasing number of detecting channels, but when over 10 channels, the degree of optimization becomes gradually not obvious.

From all elite individuals reconstructed with different number of channels, the mean of standard error (S.E.) curves shown in figure 18 and standard deviation (S.D.) curves these elite group can easily be saved by the iteration program.

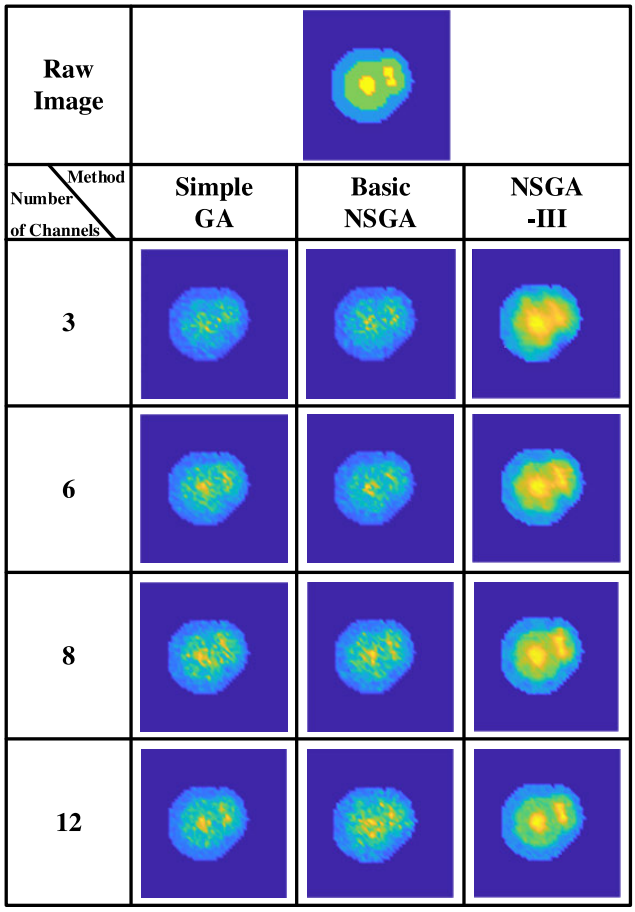

FIGURE 15. Comparison of reconstructive results between GA, NSGA and NSGA-III with same virtual data, and different number of channels.

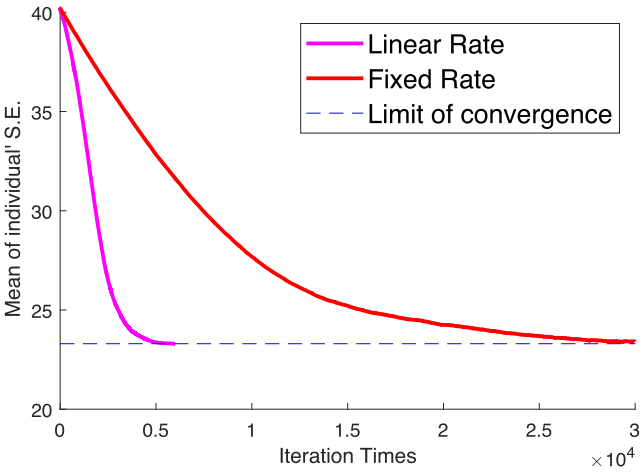

FIGURE 16. Comparison between tests with different mutation rate.

All S.E. and S.D. were generated by a solitary program which compare the current results with the original artificial data as figure 17(a) during the iteration, and have no influence on accuracy in the iteration process.

In figure 19, the S.D. value of elite individuals' S.E. means that, based on the proposed ambient pressure operator,

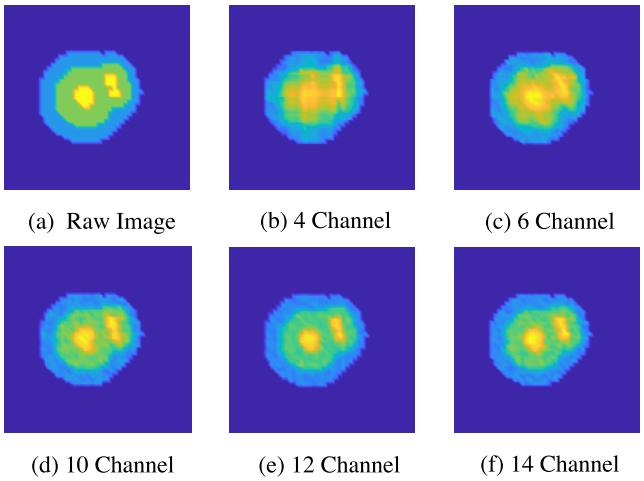

FIGURE 17. Comparison between reconstructive results with 4-14 channels under same conditions.

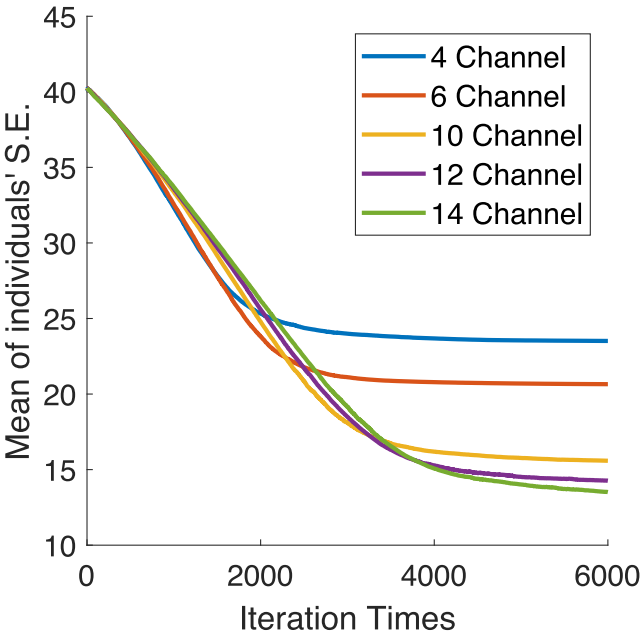

FIGURE 18. Mean value of elite individuals' S.E. calculated by different number of channels in the iteration.

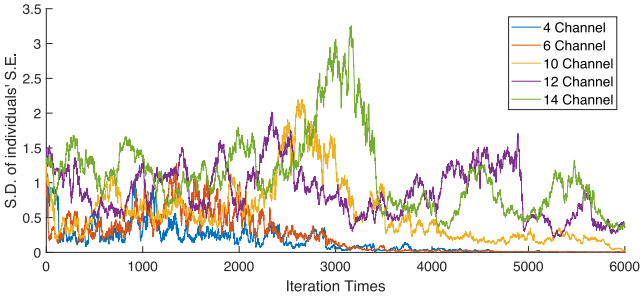

FIGURE 19. S.D. value of elite individuals' S.E. calculated by different number of channels in the iteration.

the iteration process can keep a stable group diversity, and avoid local optimization in some degrees.

In the meanwhile, the mean S.E. curves in figure 15 indicates that the more number of channels, the better

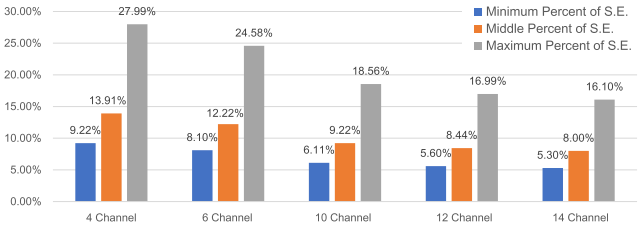

FIGURE 20. Comparison of percentage of S.E. with different number of channels.

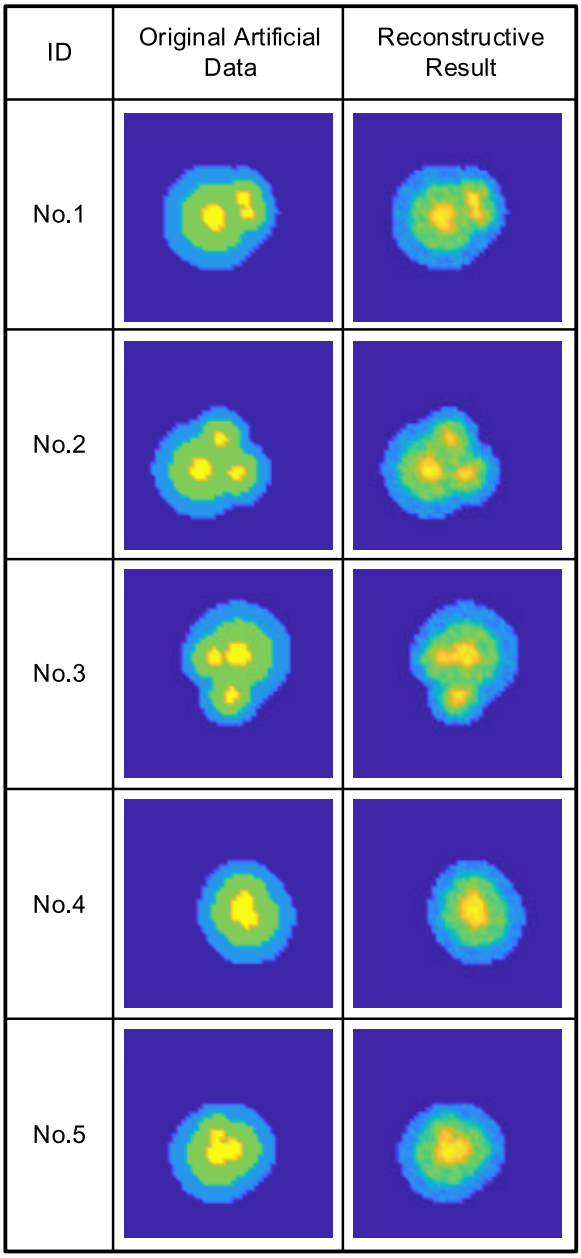

FIGURE 21. Different reconstructive results of different targets with 10 detecting channels.

reconstructive results. However, the more number of channels means the higher cost of calculating time. So, considering the artificial data only have three set value(i.e. 84, 169, and 255),

the percentage of S.E. to the truth value (i.e. artificial data as figure 17(a)), was introduced to evaluate the reconstructive results with different number of channels as figure 20.

Considering the visible results in figure 14, the S.E. curves in figure 15, and the time cost, 10 or 12 channels are recommended in this proposed reconstructive theory. The first reason is, as figure 14(b) and (c), the reconstructive results figure 17, the reconstructive accuracy rise slowly but pay a high time cost in computation.

D. COMPARISON BETWEEN DIFFERENT TARGETS

The same number of detective channels and different virtual 2-D fireball data were used to prove the fitness of the reconstructive method when dealing with different targets. Over 30 artificial data were used in this simulation, and the results were all basically meet our expectations, five of our reconstructive results is shown as figure 21.

The relative mean value curves of elite individuals' S.E., generated by different artificial fireball data with 10 same detecting channels, are shown in figure 22, from which all targets can be observed converging to a similar S.E. value.

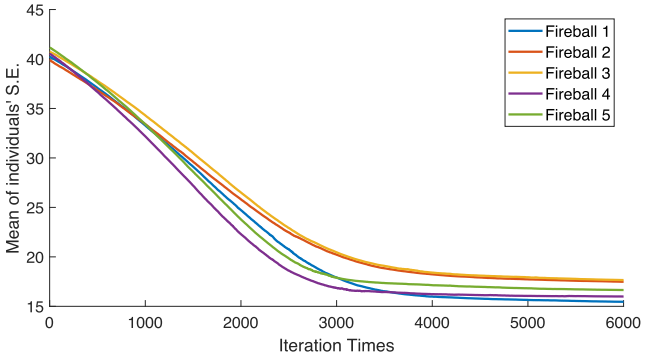

FIGURE 22. In region S.E. mean curves of different targets.

E. ALGORITHM STABILITY

Finally, all parameters were set in the same to conclude the repeatability of the proposed reconstructive method. The result is described in figure 23, in which the same number of channels can finally converge to the same S.E. value. However, the results also indicate that different number of channels may lead to a different converging results, the same as the results in subsection 3.2.

IV. CONCLUSION

The introduction of MOOP can solve the fireball-field reconstructive problem, and the reconstructive results of NSGA-III is much better than those without using NSGA theory. From the guide of the 2-D reconstructive results, 10 channels will primarily be used in the construction of detecting system. In addition, there are four advantages when implement NSGA-III in fireball-field reconstruction.

Firstly, this reconstruction theory we considered is suitable for different size of artificial data and 3-D reconstruction

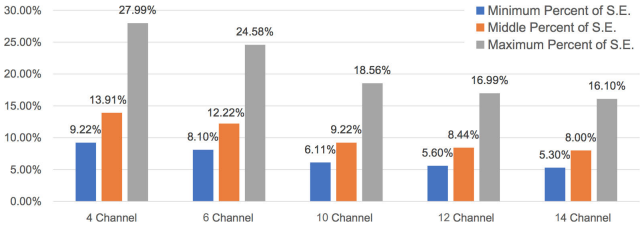

FIGURE 23. Rapid reconstructive experiments of 6 and 10 detecting channels.

problem. The different size of artificial data may reduce the accuracy of reconstruction, but which can be solved by adding the number of pixels in detecting channel. In the meanwhile, there are two differences between 2-D and 3-D reconstruction, the rising of dimension and the change of OTF. All differences are suitable for the reconstructive theory and can easily be realized when programming. What needs to be stated in advance is the reason why the smallest size of 2-D artificial data (i.e. a 50×50 real matrix) was used in simulation experiments above, is reducing the computational period while calculating the high-dimensional MOOP by NSGA-III.

To the second, different from general computed tomography (CT), only forward relative equations are needed in the reconstructive system. Difficulty of operation can be reduced because that backward equations or solutions of the forward relative equations are not needed in the algorithm.

To the third, the limitation of iterated area by an accessible method (e.g. surface reconstructive method in 3-D condition) does have a better reconstructive result than Jakub's in the iteration. This may because the limitation can reduce the risk of correction value being distributed to the nodes outside the correct region while performing GA manipulation.

To the fourth, the use of ambient pressure operator based on the D-value between detecting value and calculated value of each unit in one detecting channel, can limit the mutation rate in a reasonable range as figure 16, keeping both the individuals' similarity to the mean of back-projections, and the diversity of the elite group.

This is our first trial in using NSGA-III to solve field reconstruction problem based on many objective optimization which means there are still many works to do in the future. The iteration results and the performance of our algorithm can merely satisfy our primary needs, and whether this method is suitable to other complicated problem should be answered very precisely. Two main weaknesses in our research are as below.

Firstly, from both the reconstruction results and the iteration curves, we believe that the algorithm can be further optimized for better results and smaller error. The niche-preservation approach should be considered and the balance of convergence and diversity should be kept better. We plan to seek the solution to the limitation and weakness in this field-reconstruction problem by the above two significant points.

Secondly, We do agree with the idea that, whether the modified algorithm could achieve better performance than other state-of-the-art algorithms, should be tested on benchmark problems and using some statistical analysis as is mentioned in paper [25], which gives us a great idea to make our work more credible.

Finally, What to do in the future are the regularization of algorithm, the implement of real OTF and the rising of dimension(i.e. from 2-D simulation to 3-D simulation).

ACKNOWLEDGMENT

The authors would like to thank all reviewers and relative people for their constructive remarks and useful suggestions, which improve the work significantly.

REFERENCES

[1] R. Patra and P. K. Dutta, "Parametric reconstruction of diffuse optical tomography using Gaussian mixture model and genetic algorithm," *IEEE J. Sel. Topics Quantum Electron.*, vol. 22, no. 3, pp. 58–68, May 2016.
[2] X. Yuan, H. Tian, Y. Yuan, Y. Huang, and R. M. Ikram, "An extended NSGA-III for solution multi-objective hydro-thermal-wind scheduling considering wind power cost," *Energy Convers. Manage.*, vol. 96, pp. 568–578, May 2015.
[3] X. Bi and C. Wang, "An improved NSGA-III algorithm based on elimination operator for many-objective optimization," *Memetic Comput.*, vol. 9, no. 4, pp. 361–383, Jul. 2017.
[4] F. Li, "Analysis of atmospheric transmission impact on mid-wave and long-wave infrared radiation," (in Chinese), *Infr. Technol.*, vol. 41, no. 4, pp. 1001–8891, May 2019.
[5] M. M. Hossain, G. Lu, D. Sun, and Y. Yan, "Three-dimensional reconstruction of flame temperature and emissivity distribution using optical tomographic and two-colour pyrometric techniques," *Meas. Sci. Technol.*, vol. 24, no. 7, Jun. 2013, Art. no. 074010.
[6] Y.-W. Li, H.-Y. Yuan, Y. Lu, R.-F. Xu, M. Fu, M. Yuan, and L. Han, "Experimental studies of electromagnetic wave attenuation by flame and smoke in structure fire," *Fire Technol.*, vol. 53, no. 1, pp. 5–27, Jan. 2017.
[7] T.-J. Li, S.-N. Li, Y. Yuan, F.-Q. Wang, and H.-P. Tan, "Light field imaging analysis of flame radiative properties based on Monte Carlo method," *Int. J. Heat Mass Transf.*, vol. 119, pp. 303–311, Apr. 2018.
[8] X. Wang, Z. Wu, Z. Zhou, Y. Wang, and W. Wu, "Temperature field reconstruction of combustion flame based on high dynamic range images," *Opt. Eng.*, vol. 52, no. 4, Apr. 2013, Art. no. 043601.
[9] I. Das and J. E. Dennis, "A closer look at drawbacks of minimizing weighted sums of objectives for Pareto set generation in multicriteria optimization problems," *Struct. Optim.*, vol. 14, no. 1, pp. 63–69, Aug. 1997.
[10] A. Metiaf, Q. Wu, and Y. Aljeroudi, "Searching with direction awareness: Multi-objective genetic algorithm based on angle quantization and crowding distance MOGA-AQCD," *IEEE Access*, vol. 7, pp. 10196–10207, Jan. 2019.
[11] O. Giustolisi and D. A. Savic, "Advances in data-driven analyses and modelling using EPR-MOGA," *J. Hydroinform.*, vol. 11, nos. 3–4, pp. 225–236, Jul. 2009.
[12] H. Li and Q. Zhang, "Multiobjective optimization problems with complicated Pareto sets, MOEA/D and NSGA-II," *IEEE Trans. Evol. Comput.*, vol. 13, no. 2, pp. 284–302, Apr. 2009.
[13] F. Ruan, R. Gu, T. Huang, and S. Xue, "A big data placement method using NSGA-III in meteorological cloud platform," *EURASIP J. Wireless Commun. Netw.*, vol. 2019, no. 1, Jun. 2019, 143.
[14] S. Dhanalakshmi, S. Kannan, K. Mahadevan, and S. Baskar, "Application of modified NSGA-II algorithm to combined economic and emission dispatch problem," *Int. J. Electr. Power Energy Syst.*, vol. 33, no. 4, pp. 992–1002, May 2012.
[15] S. Carlucci, G. Cattarin, F. Causone, and L. Pagliano, "Multi-objective optimization of a nearly zero-energy building based on thermal and visual discomfort minimization using a non-dominated sorting genetic algorithm (NSGA-II)," *Energy Buildings*, vol. 104, pp. 378–394, Oct. 2015.
[16] C. Z. Cooley, M. W. Haskell, S. F. Cauley, C. Sappo, C. D. Lapierre, C. G. Ha, J. P. Stockmann, and L. L. Wald, "Design of sparse Halbach magnet arrays for portable MRI using a genetic algorithm," *IEEE Trans. Magn.*, vol. 54, no. 1, pp. 1–12, Jan. 2018.
[17] J. Bielecki, "A genetic algorithm-based method of neutron emissivity tomographic inversion for tokamak plasma," *Fusion Eng. Des.*, vol. 127, pp. 160–167, Feb. 2018.
[18] M. Merras, A. Saaidi, N. El Akkad, and K. Satori, "Multi-view 3D reconstruction and modeling of the unknown 3D scenes using genetic algorithms," *Soft Comput.*, vol. 22, no. 19, pp. 6271–6289, Oct. 2018.
[19] J.-H. Yi, S. Deb, J. Dong, A. H. Alavi, and G.-G. Wang, "An improved NSGA-III algorithm with adaptive mutation operator for big data optimization problems," *Future Gener. Comput. Syst.*, vol. 88, pp. 571–585, Nov. 2018.
[20] S. Jafar-Zanjani, S. Inampudi, and H. Mosallaei, "Adaptive genetic algorithm for optical metasurfaces design," *Sci. Rep.*, vol. 8, no. 1, pp. 1–16, Jul. 2018.
[21] F. M. Elahe, "Extraction of decision alternatives in construction management projects: Application and adaptation of NSGA-II and MOPSO," *Expert Syst. Appl.*, vol. 39, no. 3, pp. 2794–2803, Feb. 2012.
[22] I. Das and J. E. Dennis, "Normal-boundary intersection: A new method for generating the Pareto surface in nonlinear multicriteria optimization problems," *SIAM J. Optim.*, vol. 8, no. 3, pp. 631–657, Aug. 1998.
[23] Z. Cui, Y. Chang, J. Zhang, X. Cai, and W. Zhang, "Improved NSGA-III with selection-and-elimination operator," *Swarm Evol. Comput.*, vol. 49, pp. 23–33, Sep. 2019.
[24] X. Bi and C. Wang, "A niche-elimination operation based NSGA-III algorithm for many-objective optimization," *Int. J. Speech Technol.*, vol. 48, no. 1, pp. 118–141, Jan. 2018.
[25] J. Derrac, S. García, D. Molina, and F. Herrera, "A practical tutorial on the use of nonparametric statistical tests as a methodology for comparing evolutionary and swarm intelligence algorithms," *Swarm Evol. Comput.*, vol. 1, no. 1, pp. 3–18, Mar. 2011.

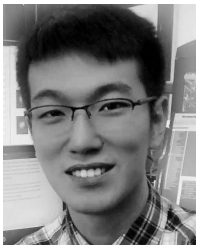

XUE BING received the B.S. degree in measurement and control technology and instruments from the North University of China, Shanxi, China, in 2017. He is currently pursuing the M.S. degree in instrument science and technology. His research interests include back-end data processing, multi-objective optimization problem, high-temperature detecting theory, and three-dimensional field reconstructive systems.

HAO XIAOJIAN received the B.S. degree in testing technology from the Department of testing technology, Taiyuan Institute of Machinery, Shanxi, China, in 1991, the M.S. degree in measurement technology and instruments from the North China Institute of Technology, Shanxi, in 2000, and the Ph.D. degree in measurement technology and instruments from the North University of China, Shanxi, in 2005. She was a Postdoctoral Student with the Beijing University of Technology, from 2006 to 2010. She is currently a Professor and the Secretary of the Party Committee in the School of Instrument and Electronics. Her research interests include measurement technology and instruments, optoelectronic technology, and dynamic parameter testing technology.

LIU XUANDA received the B.S. degree in electrical engineering and its automation from the North University of China, Shanxi, China, in 2018. He is currently pursuing the M.S. degree in instrument Science and technology. His research interests include front-end detection and three-dimensional high-temperature field reconstructive systems.

HAN ZIQI received the B.S. degree in measurement and control technology and instruments from the North University of China, Shanxi, China, in 2019. She is currently with the Beijing Institute of Computing and Communication. Her research interests include engineering algorithm noise reduction and algorithm optimization.

ZHOU HANCHANG received the B.S. degree in artillery design and manufacturing from the Beijing Institute of Technology, Beijing, China, in 1960. He is currently a Professor with the School of Information and Communication Engineering, Beijing Institute of Technology. He is also an Expert with special allowance from the State Council and the Leader of Photoelectric Instrument and New Sensing Technology in the Key Laboratory of Instrument Science and Dynamic Testing, Ministry of Education. His research interests include photoelectric detection theory and technology, special sensing theory and technology, and optical instruments and technology.